Dynamical liquid-gas phase transition

C. Appert, Stéphane Zaleski

Classification
Physics Abstracts
47.55K — 05.70F — 05.50

Dynamical liquid-gas phase transition

C. Appert and S. Zaleski

Laboratoire de Physique Statistique, Ecole Normale Supérieure, 24 rue Lhomond, 75231 Paris Cedex 05, France

(*Received 28 July 1992, accepted in final form 19 November 1992*)

Abstract. — We describe in detail a lattice gas model whose irreversible dynamics leads to a phase transition. Attractive and repulsive forces between particles are similar to those of our previous papers. The equilibrium properties such as the equation of state, the pressure tensor in the bulk and on interfaces, and Laplace's law are investigated numerically. Surface tension, equilibrium densities, pressure and shear viscosity are given for a catalogue of variants of the model. The surface tension is shown to vary approximately linearly : $\sigma \sim A(r - r_c)$ where r is the range of the attractive force. A critical liquid-gas point is expected at r_c. Shear kinematic viscosity varies like $\nu \sim r^2$. The equilibrium density of the gas phase decreases very rapidly with r. Equilibrium densities and pressures are also shown to vary with the curvature of the interface. The dependence on inverse radius of curvature is linear as in the Gibbs-Thomson relations, but coefficients are not identical to the thermodynamic ones. These latter results on capillary effects are in agreement with those obtained in an independent work of Pot and collaborators.

1. Introduction.

In this paper we discuss some of the hydrodynamic and thermodynamic properties of a recently introduced [1, 2] lattice gas model. This model has particles moving at discrete velocities and interacting on a discrete lattice. The motivation for the study of this lattice gas and other related models is twofold. On the one hand, it is an interesting new idea for the simulation of flow with interfaces. On the other hand, because of its irreversible microscopic dynamics, it also poses puzzling problems in statistical mechanics.

1.1 NUMERICAL SIMULATIONS OF INTERFACIAL FLOW. — Numerical simulations of interface motion in fluid flow is a problem of tremendous importance in both basic and applied sciences. Subjects range from the astrophysical, such as photon bubbles in the sun, to the countless industrial processes that involve multiple phase flow. In some cases, such as the Kelvin Helmholtz instability, the addition of viscosity to the inviscid problem increases its complexity from the almost rigorously solvable to a frustrating degree of complexity.

The most difficult problem faced by the numerous numerical methods devised so far [3] are the changes of topology that the interfaces may undergo. A picture of the type of reconnection configuration we have in mind is shown in figure 1. Even in two dimensions of space these

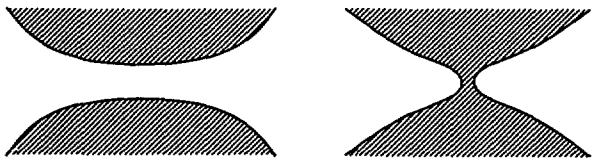

Fig. 1. — Interface reconnection.

problems may be daunting. It seems that the potential user of numerical methods is facing a dilemma :

(i) either to use accurate methods such as front tracking [4], but facing difficult problems with reconnection, especially if mass and momentum conservation is required ;

(ii) or to use front capturing methods such as Volume Of Fluid [5]. These methods attribute an amount of volume of each fluid to cells regularly located on the lattice. They thus keep track of mass transfers between cells, and thus make reconnection spontaneous. However they are plagued with other difficulties such as a slow degradation of the interface in the flow [6].

An additional difficulty that we have not yet mentioned is that the fluid equations themselves do not prescribe when reconnection should happen in 2D flow. Reconnection is in fact obtained after a potential barrier is crossed, usually thanks to thermal motion. This situation is nicely evidenced in experiments on 2D films [8]. Perhaps the only satisfactory treatment of the reconnection problem is to use molecular dynamics [7], using adequate interparticle potential and thus reconstructing realistic potential barriers. However, such calculations are of formidable cost if a large range of scales is required.

The possibility of simulating interfaces with lattice gases [9] allows a completely new treatment of this type of problem. In fact, it is no longer an entirely new subject [10]. In 1988 Rothman and Keller [11] proposed an immiscible lattice gas (ILG) model. It simulates binary fluids, in which two species of particles coexist on the lattice. Interactions between nearest neighbors sites ensure spontaneous separation of the two phases. Other lattice gas models bring into play reactive collisions [13, 14] or minimal diffusion [12].

The liquid-gas model which we introduced before [1, 2] and study in detail in this article is distinguished from the previous ones by the presence of a single species of particles. These separate into a dense and a light phase. The light phase is somewhat similar to the ordinary lattice gas, while the dense phase has large deviations from the gas equation of state and may rather be called a « liquid » lattice gas (LLG).

Models such as the ILG and LLG satisfy the requirements we set above :

(i) they conserve mass ;

(ii) interfaces form spontaneously during spinodal decomposition, and are not destroyed as simulation time advances.

They are a kind of simplified molecular dynamics ; as such they may offer an interesting intermediate level of analysis between macroscopic and microscopic scales.

Lattice gases have other, intrinsic advantages for the simulations of some interfacial flows. The molecular noise which is a detriment in certain situations becomes an advantage in situations where it actually contributes to interface breaking. For instance, the Brownian motions of droplets is an important feature for the understanding of domain growth dynamics. Spinodal decomposition is in fact much more realistically simulated by methods which involve noise, such as the lattice gas, than by methods which avoid it, such as the Boltzmann lattice gas [17].

1.2 STATISTICAL MECHANICS OF IRREVERSIBLE SYSTEMS. — The other motivation for the study of interacting lattice gases comes from statistical mechanics. An important feature of LLG and ILG models is that the interaction step is not a reversible transformation of the set of configurations of the lattice. This makes the model inherently different from classical models for the dynamics of phase transition such as Monte Carlo or microcanonical [18] simulations of the Ising model. This difference is a profound one that affects the thermodynamics and statistical mechanics of the model.

In these classical models, the state of a model, i.e. the probability distribution $P(S)$ of all configurations S on the lattice is given by Gibbs distributions :

$$P(S) = \exp(-\beta E_S) \tag{1}$$

where the energy E_S is a function of the state S and β is the inverse temperature. All the machinery of statistical physics may be obtained from the existence of the invariant measure $P(S)$. In particular, a free energy $F(\beta)$ may exist in the thermodynamic limit, and its minimization allows to investigate the thermodynamic equilibrium. Phase separation may then be interpreted in terms of such a free energy. In particular, basic thermodynamic results about interfaces between phases in equilibrium such as the equality of chemical potentials accross phase boundaries results from the minimization of F.

In irreversible lattice gas models, the invariant measure is not known *a priori*. The large scale behavior of the system may however be in part inferred from symmetries and conservation laws, and in part from an approximation of the true invariant measure, based on the idea of Boltzmann molecular chaos — or factorization. In particular, the factorization idea allows to predict, albeit only approximately, the existence of a phase transition and the critical value of the parameters for which it occurs. This prediction has been performed for two color models [19] as well as one color models [1].

To emphasize the role of irreversibility, let us consider the classical entropy of a fermionic system such as the lattice gas. Its value for the entire lattice is maximized for homogeneous distributions $P(S)$. Only if the second principle is somewhat invalidated can a phase transition be observed in our irreversible systems. In yet other words, the irreversible dynamics selects an attractor in phase space of smaller volume than the region accessible to ergodic, reversible models.

The question then arises of the nature of the constraints that replace the thermodynamic ones for our systems. The symmetries of the system go a long way towards predicting its large scale features. For instance, most capillary effect do not, in fact, require classical thermodynamics. They may be obtained in a purely mechanical way for a system where momentum is conserved. However there are other « purely thermodynamic » constraints on interfaces, such as the equality of chemical potentials that may not be predicted from conservation laws and symmetries alone.

Perhaps the most interesting question is to determine what general laws are applicable to irreversible particle systems. What are the differences and the similarities with classical thermodynamics and statistical mechanics ? Even an introductory discussion of this topic would be beyond the scope of this paper, but we may suggest two typical problems. One is the universality of the scaling properties of phase transitions. Are critical exponents for irreversible systems in the same universality classes as those of reversible systems ? Another question concerns thermodynamics : is there an effective free energy that would replace the Gibbs free energy for irreversible systems ?

In this article we choose to concentrate on the thermodynamic rather than the statistical mechanical aspects *per se*. The issue of thermodynamics for our systems is of the greatest importance for their applications. Moreover, our model is in some sense a minimal model for

non trivial thermodynamics of interfaces. Indeed, a non-trivial consequence of the equality of thermodynamic potentials are the Gibbs-Thomson relations (Eq. (12) below). These are irrelevant in simpler models where the two phases are symmetrical such as the binary fluid ILG.

2. Interacting lattice gas models.

In this section we introduce a number of variants of the lattice gas model. All our models are constructed on top of the FHP models [9, 22]. Let us first recall the basic rules for these models. We will discuss in this work models with two dimensions of space only (possible extension to 3D was pointed out in [20]). They model fluids as systems of fictitious particles moving on a hexagonal lattice.

Each particle has one of seven possible velocities. Six are identical to the unit vectors $\mathbf{c}_i$ of the lattice

$$\mathbf{c}_i = \left(\cos\frac{\pi(i-1)}{3}, \sin\frac{\pi(i-1)}{3}\right) \qquad 1 \leqslant i \leqslant 6$$

and $\mathbf{c}_0 = 0$. The lattice is the set of points $\mathbf{x}_{ij} = i\mathbf{c}_1 + j\mathbf{c}_2$.

An exclusion principle is imposed : no more than one particle may have a given velocity on any one node. In other words, the configuration of a site can be represented by a Boolean vector $s = (s_i(\mathbf{x}, t),\ 0 \leqslant i \leqslant 6)$ where $s_i = 0$ or 1. On any given site $\mathbf{x}$ the number of particles is $p = \sum_{i=0}^{6} s_i$ and the momentum is $\mathbf{g} = \sum_{i=1}^{6} s_i\,\mathbf{c}_i$. The system evolves by the succession of two steps : the propagation and collision steps that conserve momentum and mass locally. These steps are pictorially described in figure 2. During propagation, particle s_i hops by one lattice unit in the direction $\mathbf{c}_i$. In the collision step particles on a given node exchange mass and momentum according to rules which are either strictly deterministic or partially stochastic. A few examples of collisions are shown in figure 2. Among the now classical models, we use FHP III ([1]) with some minor changes.

In the present model, an interaction between particles is added to the evolution process. In the interaction step, we model an attractive force between particles on distinct sites. The exertion of a force on a site is nothing else than the addition of momentum to it. The interaction between sites may then be represented by the exchange of a quantity $\mathbf{t}$ of momentum between the sites. The effect of this addition is to send particles initially flying away from each other back towards each other. Let $\mathbf{x}_a$, $\mathbf{x}_b$ be the two interacting sites, and $\mathbf{g}_a$, $\mathbf{g}_b$ their momenta before the interaction. Then after the interaction, the new momenta are $\mathbf{g}_a + \mathbf{t}$, $\mathbf{g}_b - \mathbf{t}$. Examples are shown in figure 4. As we shall see below, the addition of the interaction results in a modified equation of state, leading to the formation of interfaces in the lattice gas, our stated goal.

To make our idea more precise, we need to define how much momentum is exchanged and in what order we explore the pairs. Two possible directions may be followed at this stage. The first one is to exchange the largest $|\mathbf{t}|$ without violating conservation laws. In particular, the number of particles on each site is conserved. This leads to so called « maximal interaction » models, and makes the rule in some sense optimally efficient. It is the route followed in reference [2]. However the order in which pairs are explored is then non trivial as we shall see. Thus it may be advantageous to explore another direction : exchange a relatively small amount of momentum by considering only the first interaction of figure 4. The interaction is performed

([1]) In fact the collision rules we used are slightly different from those of the FHP III model. See Appendix A for more details.

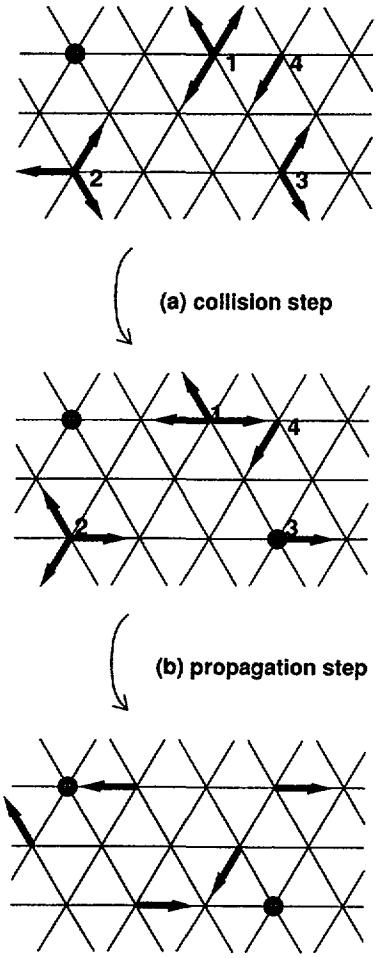

Fig. 2. — Collision and propagation on a triangular lattice. a) Particles are represented before their collisions and after. Small circles represent particles at rest, with 0 momentum. Labels 1 and 2 refer respectively to two and three body collisions. Label 3 shows a collision involving a rest particle. Notice that each collision conserves total momentum. Some sites are left unchanged as there is no possible redistribution of particles that conserves momentum (label 4). b) Propagation of particles is shown. Each particle advances by one step in the direction of its momentum. Boundary conditions are either periodic or explicitly defined in the text.

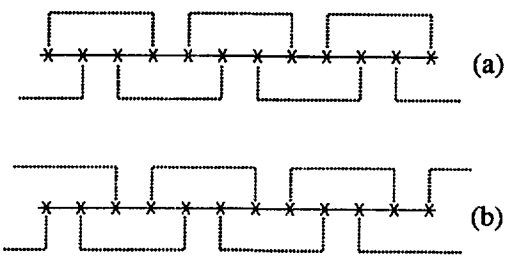

Fig. 3. — Pairs of interacting sites. Only one line of the lattice has been represented. (a) « even » pairs, (b) « odd » pairs.

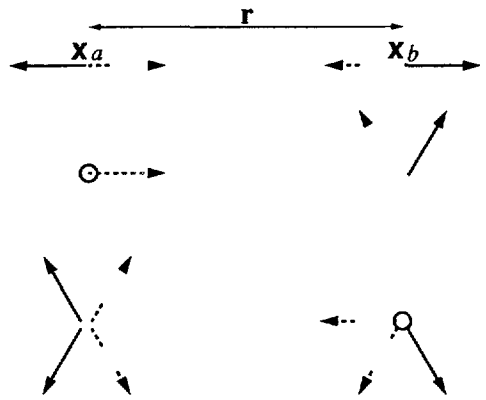

Fig. 4. — Examples of attractive interaction rules. Only the two interacting sites are represented. The states occupied before and after the interaction are represented respectively by solid and dotted lines. Only the top interaction is performed in the minimal model.

for any given pair only if the directions in full lines are occupied before any interactions occur and the directions in dashed lines are empty. The interesting point about this rule is that, although the average exchanged momentum $|\mathbf{t}|$ is smaller, all pairs can be explored in parallel. This « minimal interaction » route has been followed in reference [20]. In what follows we report on numerical simulations following the « maximal interaction » ideas. However, we still sometimes refer to the minimal model, for which a fuller theoretical understanding is available.

Let us describe the maximal model more precisely. The distance r between interacting sites is fixed once and for all. Thus only sites at this given distance interact, a feature of the model for which our main excuse is the sake of simplicity : at each time step, particles hop and collide according to the usual lattice gas rules. Then we perform the interaction on all pairs of sites at distance r in a predefined order. At each time step, we select at random one of the 3 directions of the lattice, i.e. one of the directions parallel to either $\mathbf{c}_1$, $\mathbf{c}_2$ or $\mathbf{c}_3$. Naturally, we label these directions by the corresponding indexes $1 \leqslant k \leqslant 3$. Interactions are performed only in that direction. For « horizontal » pairs ($k = 1$) we define « even » pairs as those of the form $(\mathbf{x}, \mathbf{x} + r\mathbf{c}_1)$ with $\mathbf{x} = 2i\mathbf{c}_1 + j\mathbf{c}_2$. All even pairs may be explored independently for interactions, in other words, the outcome of the interaction step does not depend on the order in which the pairs are explored. After all the « even » pairs are explored, we investigate the « odd » pairs that complement the set of horizontal pairs. The division in even and odd pairs is shown in figure 3. Such a simple splitting of the set of pairs is possible only for odd distances r. Non-horizontal pairs are explored similarly.

The amount of momentum exchanged between pairs may depend on the variant chosen for the model. However, a general rule is that the addition of momentum always conserves the number of particles in each site, $p(\mathbf{x})$ and $p(\mathbf{x} + r\mathbf{c}_k)$, and the total momentum of the pair $\mathbf{g}(\mathbf{x}) + \mathbf{g}(\mathbf{x} + r\mathbf{c}_k)$. Let $\mathbf{g}'$ be the momentum after interactions. The exchanged momentum is $\mathbf{t}_k = \mathbf{g}'(\mathbf{x}) - \mathbf{g}(\mathbf{x}) = \mathbf{g}(\mathbf{x} + r\mathbf{c}_k) - \mathbf{g}'(\mathbf{x} + r\mathbf{c}_k)$. The interaction is attractive if $\mathbf{t}_k \cdot \mathbf{c}_k > 0$ and repulsive if $\mathbf{t}_k \cdot \mathbf{c}_k < 0$. Examples of such interactions are shown in figure 4.

The description we have given above is only an approximation to the actual procedure used in choosing the pairs. In practice, the interaction directions for the three next steps are chosen by permuting randomly the three directions $\mathbf{c}_1$, $\mathbf{c}_2$, and $\mathbf{c}_3$ every three time steps. Homogeneity and isotropy impose additional subtle constraints on the way of defining pairs. These are discussed in appendix B.

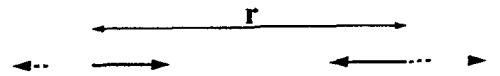

Fig. 5. — Example of a repulsive interaction. Representation conventions are the same as in figure 4.

Table I. — *Some possible variants of the maximal interaction model.*

Model	characteristics
A	The interaction is performed whenever it is possible
B	The interaction is attractive if $n > 2$ and repulsive otherwise. n is the total number of particles in the pair.
C	The interaction is performed only if $n > 4$

The basic rule for determining **t** is to exchange as much momentum as possible. However, variants of the model with more elaborate rules have been developed. In these variants, **t** depends on the number of particles in the pair. This allows some flexibility in the equation of state and equilibrium densities. Table I gives the list of those mentioned in this paper. The spinodal decomposition of figure 6 has been obtained with variant *C*, which has higher equilibrium densities than the basic form A of the model.

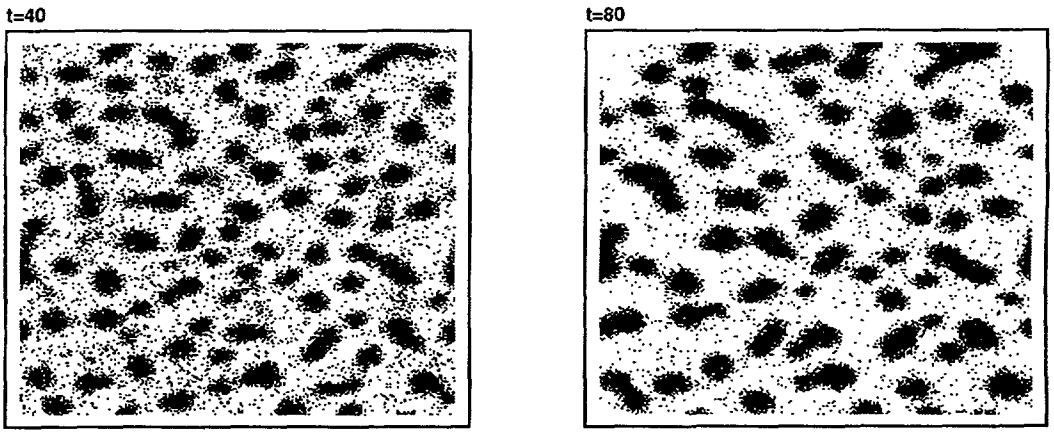

Fig. 6. — Spinodal decomposition obtained with variant *C*, $r = 5$. The $240 \times (240\ \sqrt{3}/2)$ lattice is initialised with a uniform density $d = 0.2$ particle per site.

The decomposition observed in our simulations indeed follows the picture given by Landau and Lifshitz [25] for the change from a metastable to a stable phase. In a homogeneous medium, fluctuations form small quantities of a new phase, or nuclei. As the creation of an interface is an energetically unfavourable process, only nuclei whose size is above a certain critical value are stable ; other nuclei disappear again. The dissolution of small droplets or bubbles and the growth of larger ones occur indeed in our simulations (Fig. 7). We also

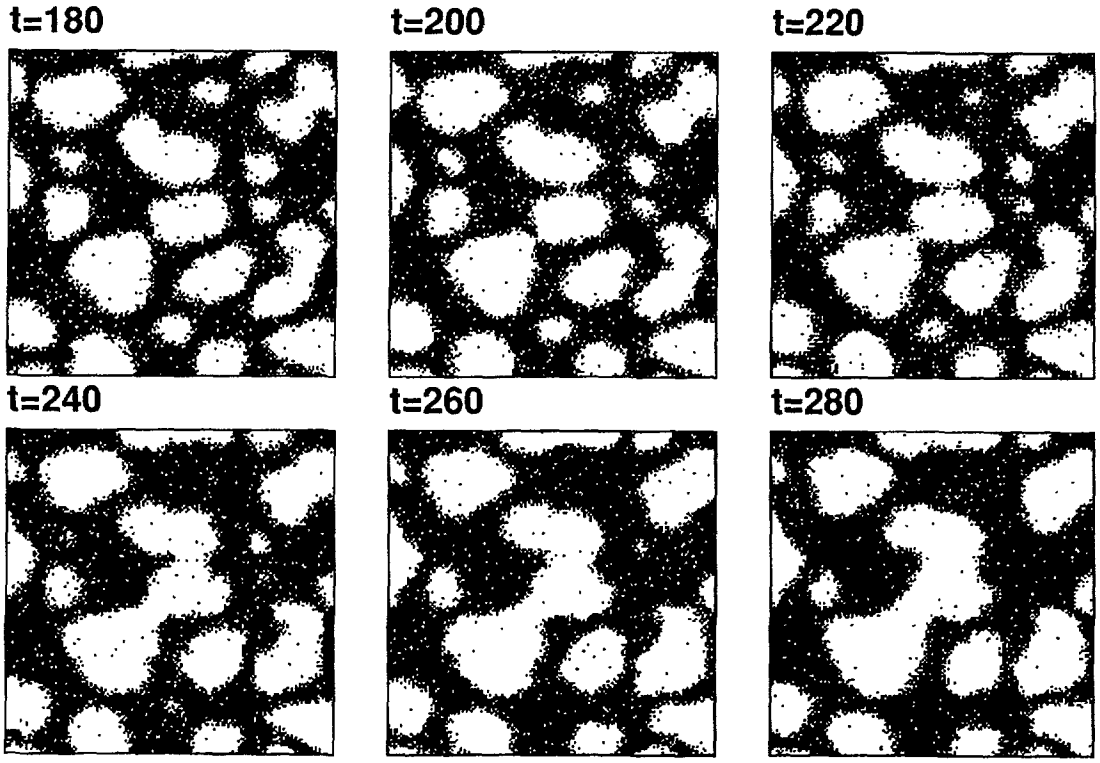

Fig. 7. — Dissolution of bubbles and breaking of links. We show only one part 120 × 120 of the lattice. Model A has been used with $r = 3$ and a uniform initial density $d = 0.3$.

observe some other mecanisms for the growth of domains, such as the breaking of links. Figure 8 illustrates the symmetric process, the coalescence of droplets.

Simulations have been carried out on a SPARC 2 Sun Workstation. The frequency of updates is then between 80 000 and 100 000 nodes per second. On a HP 730 computer, the code reaches 130 000 nodes per second. The configuration of a site is represented by a Boolean vector. Propagation, collision and interaction operators are coded making extensive use of table look-up algorithms.

3. Invariants.

Our model has the usual particle number and momentum invariants

$$\mathbf{N} = \sum_{\mathbf{x}} \sum_{i} s_i(\mathbf{x}) \tag{2}$$

$$\mathbf{G} = \sum_{\mathbf{x}} \mathbf{g}(\mathbf{x}) . \tag{3}$$

In addition to these invariants, the FHP model is known to have spurious invariants [21]

$$J^k(t) = \sum_{\mathbf{x}} (-1)^{t+j_k} \mathbf{g}(\mathbf{x}) \cdot (\mathbf{c}_{k+1} + \mathbf{c}_{k+2})$$

with

$$j_k = \frac{4}{3} \mathbf{x} \cdot (\mathbf{c}_{k+1} + \mathbf{c}_{k+2})$$

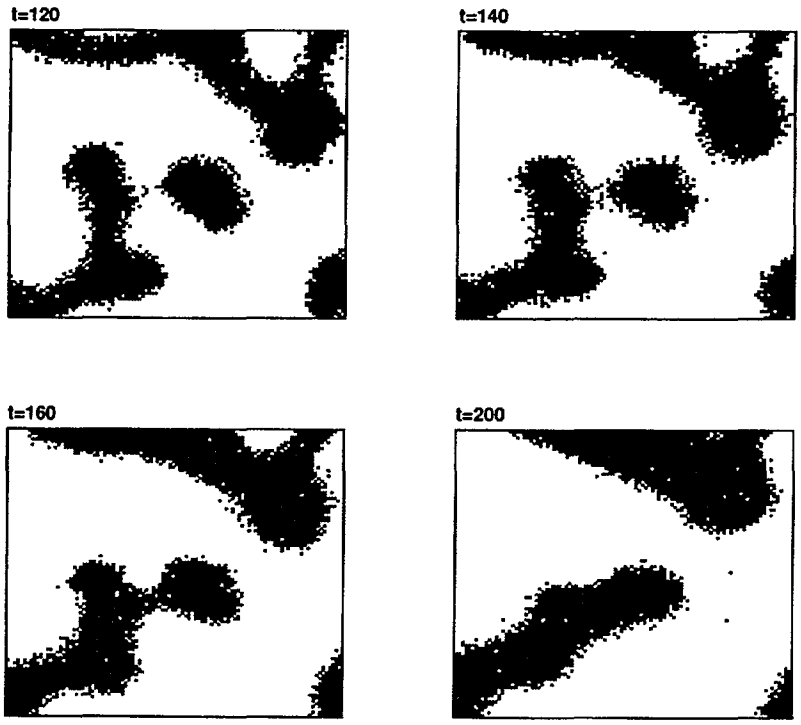

Fig. 8. — Coalescence of two droplets. We show only one part of the lattice. Model A has been used with $r = 5$. The uniform initial density is $d = 0.2$.

$k = 1$, 2, or 3. J_k is a constant of the motion for the FHP type models. This invariance may be pictured as a consequence from the exchange of momentum between odd and even lines during the propagation step. Our interacting model breaks these invariants. Indeed, interactions with an odd r couple momentum of odd and even lines. This would not be the case for even values of r and is another motivation to avoid them. However, if the invariants are no longer conserved they may become unstable and saturate at a non-zero value. Some care is required in situations susceptible of exciting the invariants, that is, when there are steep gradients. As a matter of fact, an interface can be described as a steep gradient of density. We have checked during simulations that this spurious invariant was not excited. The simulation was initialited with a half-filled box, the interface being parallel to $\mathbf{c}_1$. We measured $J^1(t)$ normalized by the number of sites at each time step (Fig. 9).

4. Pressure and equations of state.

The pressure of a non-interacting gas with a uniform density ρ is easily calculated in the case of the FHP III model [22]. One gets the equation of state of a perfect, isothermal gas

$$p = \frac{b_m}{bD}\rho \tag{4}$$

where D is the dimension of space, b_m the number of moving particles and b the total number of particles. In general, it is useful to introduce the reduced density $d = \rho/b$. For our 2D models, we have $b_m = 6$, $b = 7$. The perfect gas equation is $p = 3d$.

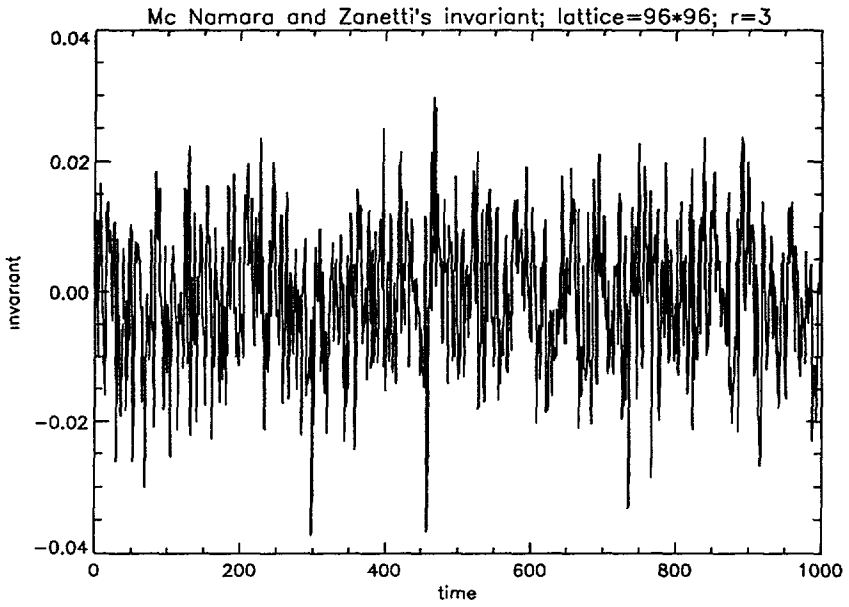

Fig. 9. — McNamara and Zanetti's invariant.

Figure 10 illustrates how attractive interactions contribute to the pressure with negative momentum transfers : we consider interactions parallel to $\mathbf{c}_k$. $\Delta\mathbf{g}$ is the momentum exchanged between the two sites. The velocity of the transfer is $-r\mathbf{c}_k$. Then the momentum transfer is $-r\mathbf{c}_k \cdot \Delta\mathbf{g}$.

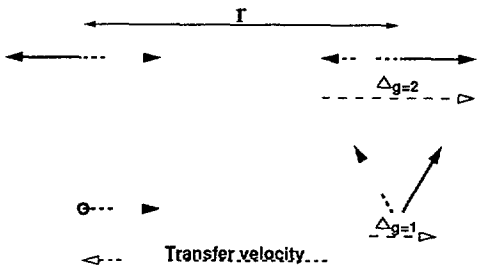

Fig. 10. — Momentum transferred during one interaction.

Let $\pi_k(\rho)$ be the average momentum transferred during one interaction step along direction $\mathbf{c}_k$:

$$\pi_k(\rho) = \langle | (\Delta\mathbf{g})_k | \rangle$$

$\pi_k(\rho)$ can be calculated from the assumption of a factorized distribution. We assume that such a distribution is realized after the propagation and collision steps. Interactions break this distribution as they introduce correlation between sites. This slightly complicates the calculation as the interaction on even pairs affect the distribution seen by the interactions on odd pairs. However, the calculation is reasonably straightforward. It is nevertheless useful to

use an electronic computer to sum over all the possible interactions for the maximal interaction model. Using the technique described in [1], [2] we obtain

$$p = 3d - r[17(d^2 + d^{12}) + 136(d^3 + d^{11}) + 571(d^4 + d^{10}) + \\ + 1\,506(d^5 + d^9) + 2\,662(d^6 + d^8) + 3\,216\,d^7]\,. \quad (5)$$

One part of the resulting equation of state is plotted in figure 11. Figure 12 shows the full curve.

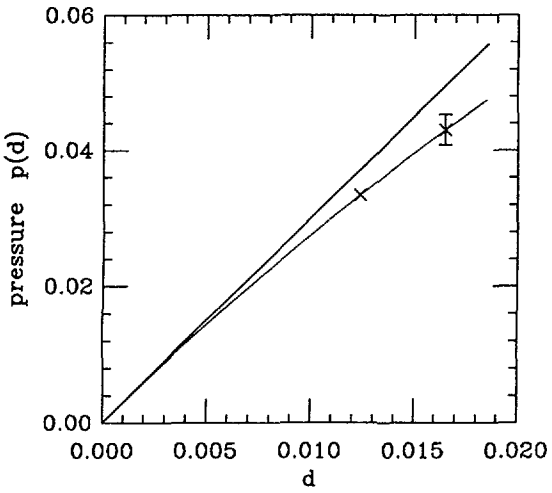

Fig. 11. — Theoretical equation of state for the maximal interaction model (dotted line) compared with numerical pressure measurements. The full line gives the equation of state for the non interacting gas.

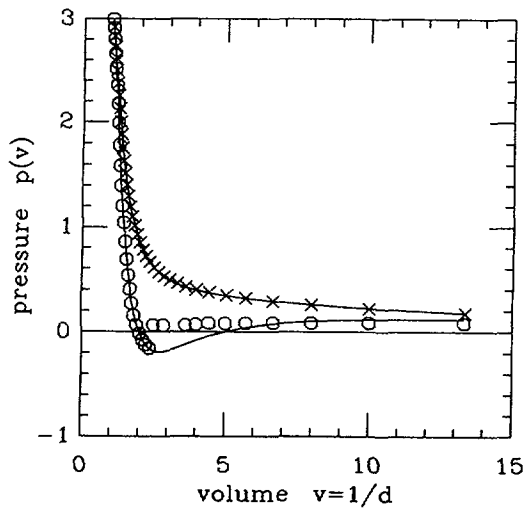

Fig. 12. — Complete equation of state for the simplified model introduced in [2]. It is an intermediate model between the maximal and the minimal model. The theoretical prediction (full line) is compared with numerical pressure measurements. Squares are numerical results for $r = 3$ and crosses are for $r = 7$. A transition is seen for $r = 7$ but not for $r = 3$.

Measurements show a fair agreement with prediction of (5). However, in the liquid phase there is no agreement within the error bars. This is to be contrasted with the situation for non-maximal models such as those of reference [1], where agreement is within statistical accuracy of the pressure measurement.

For model C we get the following equation of state :

$$p = 3d - r[1\,506(d^5 + d^9) + 2\,662(d^6 + d^8) + 3\,216\,d^7 + 571\,d^{10} + 136\,d^{11} + 17\,d^{12}]\,. \quad (6)$$

A comparison with measurements at low density is shown in figure 13.

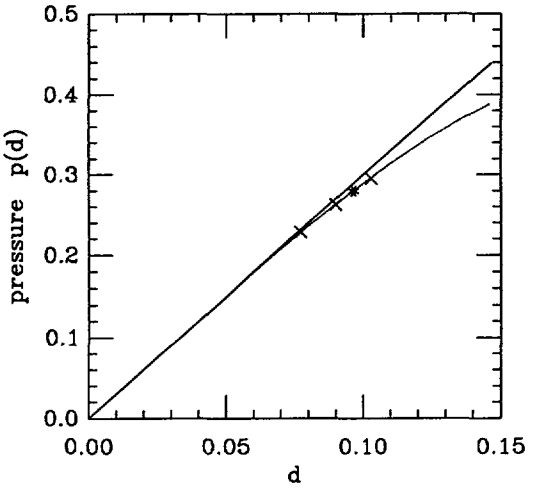

Fig. 13. — Theoretical equation of state for model C (dotted line) compared with numerical pressure measurements. The full line gives the equation of state for the non interacting gas. The star represents the equilibrium state of the gas phase.

5. Local momentum balance and pressure tensor.

It is interesting to investigate the amount of momentum transferred accross each link of the system. In FHP models this is simply the number of particles crossing the link, and the momentum transfer tensor is [22]

$$\Pi_{\alpha\beta} = \sum_i \langle s_i \rangle\, c_{i\alpha}\, c_{i\beta}\,. \quad (7)$$

In interacting models, the picture is complicated by the transfer of pressure by interactions. Let $p^{(k)}(\mathbf{x} + \mathbf{c}_k/2,\, t)$ be the momentum transferred at time t along link $(\mathbf{x},\, \mathbf{x} + \mathbf{c}_k)$. It includes the contributions of all interactions involving pairs $(\mathbf{y},\, \mathbf{y} + r\mathbf{c}_k)$ containing the link.

A local discrete balance of momentum can then be written

$$\mathbf{g}(\mathbf{x},\, t+1) - \mathbf{g}(\mathbf{x},\, t) = \sum_{k=1}^{3} [-p^{(k)}(\mathbf{x} + \mathbf{c}_k/2,\, t) + p^{(k)}(\mathbf{x} - \mathbf{c}_k/2,\, t)]\, \mathbf{c}_k\,. \quad (8)$$

Large scale averaging of (8) yields

$$\partial_t g_\alpha = - \partial_\beta \Pi_{\alpha\beta} \tag{9}$$

where

$$\Pi_{\alpha\beta} = \sum_i \langle p^{(i)} \rangle \, c_{i\alpha} \, c_{i\beta} \tag{10}$$

with the convention $\langle p^{(i+3)} \rangle = \langle p^{(i)} \rangle$.

Consider now the case of a homogeneous state. Then

$$\Pi = \begin{pmatrix} p^{(1)} + \frac{1}{4}(p^{(2)} + p^{(3)}) & 0 \\ 0 & \frac{3}{4}(p^{(2)} + p^{(3)}) \end{pmatrix}.$$

Isotropy implies $p = \Pi_{xx} = \Pi_{yy} = \frac{1}{2}(p^{(1)} + p^{(2)} + p^{(3)})$.

The transfers $p^{(k)}$ have been measured on $240 \times 240 \times \sqrt{3}/2$ lattices initially filled with a uniform density ρ. Averaging was performed on 500 time steps. The somewhat tricky programming needed to obtain the fields $p^{(k)}$ has been verified by a direct check of the balance (8). Figure 14 shows the resulting isocontours of $p^{(k)}$. We observe correlations on a range of order r in each direction. We check that although the directional transfers $p^{(k)}$ are not isotropic,

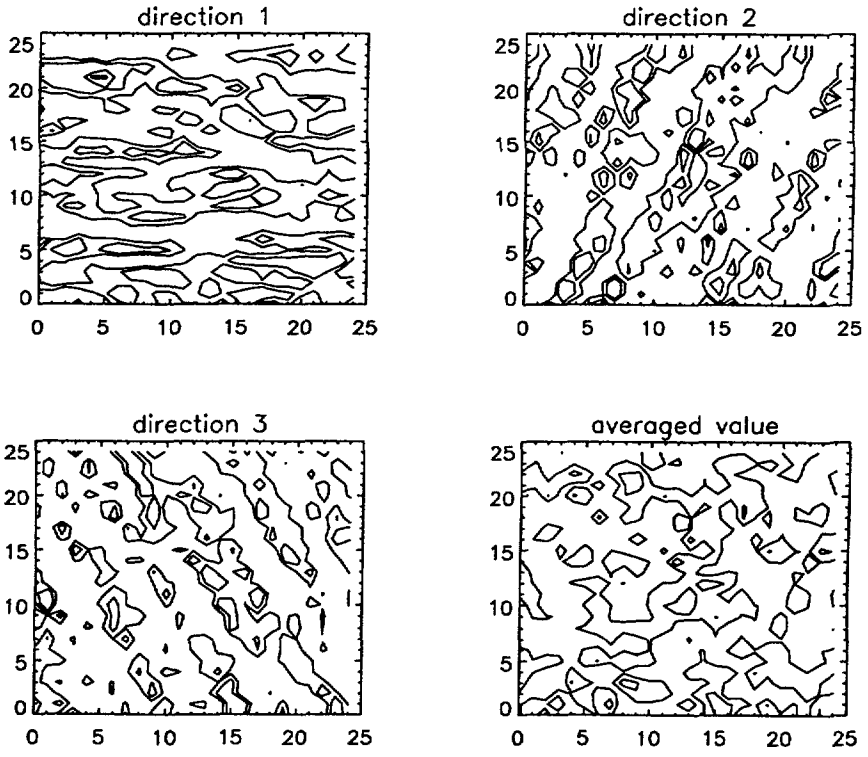

Fig. 14. — Isocontours of $p^{(1)}$, $p^{(2)}$, $p^{(3)}$, and $p = (p^{(1)} + p^{(2)} + p^{(3)})/2$.

the total pressure p has 6 fold rotational symmetry, as it should. This complements another result on the isotropy of the model : in reference [2] it has been shown that power spectra of the patterns obtained in spinodal decomposition were isotropic within statistical accuracy of the measurements.

6. Surface tension.

The behavior of an interface depends strongly on capillary phenomena. The existence of surface tension is ensured by a mechanical reasoning, as done in reference [26].

The surface tension of the interface can be defined by [26]

$$\sigma = \int_{-\infty}^{+\infty} (p_n - p_t)\, dz$$

where p is the pressure normal to the interface ; $p_n = \Pi_{\alpha\beta}\, n_\alpha\, n_\beta$, $p_t = \Pi_{\alpha\beta}\, t_\alpha\, t_\beta$ and n_α, t_α are the normal and tangential vectors to the interface. Laplace's law may be obtained from this definition [26, 24].

It is of great interest to know the values of surface tension for each variant of our models. However our approximation techniques leave us unable to predict the surface tension even in the simplest case, the minimal model [20]. We thus perform numerical measurements as described below. We have initiated simulations with a half filled box (Fig. 15). Walls limit the box at top and bottom. Boundary conditions on the right and on the left are periodic. The bottom wall attracts particles so that the dense phase stays attached to the bottom. Equilibrium is reached relatively rapidly — we have checked that for a good choice of initial densities, the transient time is negligible compared to the averaging time. Then momentum transfers along each link are counted and time averaged. Notice that here $p^{(1)}$, $p^{(2)}$, and $p^{(3)}$ depend on the coordinate z normal to the interface.

If the interface is perpendicular to $\mathbf{c}_k$: the tangential pressure is the pressure that would be exerted on a plane parallel to $\mathbf{c}_k$ (Fig. 16). For instance, for $k = 1$,

$$p_t(\mathbf{x}) = \Pi_{yy} = \frac{3}{4}\,(p^{(2)}(\mathbf{x}) + p^{(3)}(\mathbf{x}))\,.$$

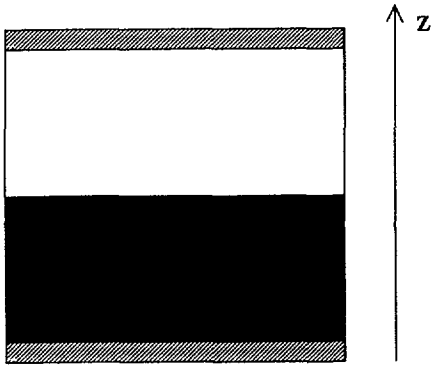

Fig. 15.

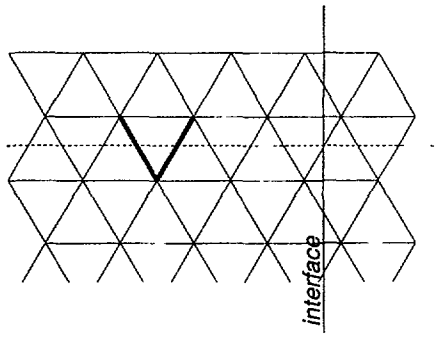

Fig. 16.

Fig. 15. — Initialization for the measurement of surface tension. The high density, low density and solid areas are represented in black, white, and grey respectively.

Fig. 16. — Links involved in normal pressure measurement. The full line is the interface and the dotted line is a fictitious plane normal to the interface. The bold links are those involved in the tangential pressure measurement at site x. (x is the site where the two bold links meet.)

The normal pressure exerted on a plane parallel to the interface is, for sites of type 1 (Fig. 17),

$$p_n(\mathbf{x}) = p^1(\mathbf{x})$$

and for sites of type 2

$$p_n(\mathbf{x}) = p^1(\mathbf{x}) + \frac{1}{2}\,[p^{(2)}(\mathbf{x}) + p^{(6)}(\mathbf{x})]$$

where $p^{(6)}(\mathbf{x}) = p^{(3)}(\mathbf{x} + \mathbf{c}_6)$.

An average along the direction parallel to the interface gives the profiles $p_n(z)$ and $p_t(z)$ (Fig. 18).

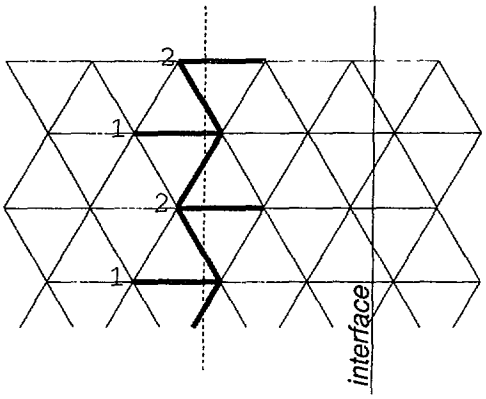

Fig. 17. — Links involved in tangential pressure measurement. The full line is the interface and the dotted line is a fictitious plane parallel to the interface. The bold links are those involved in the normal pressure measurement at sites of type 1 or 2.

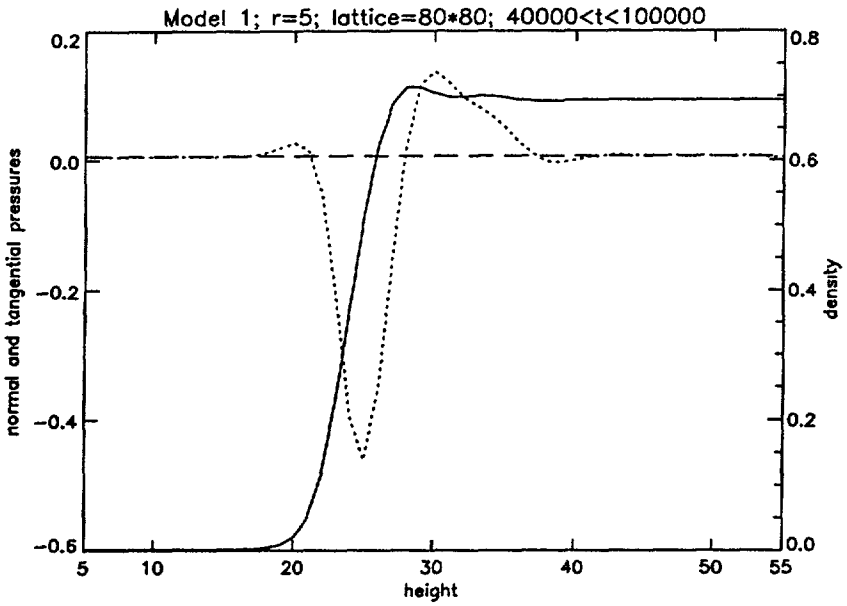

Fig. 18. — The normal (dashed line) and tangential (dotted line) pressure against the height z in the box. The full line gives the density profile.

Some other simulations have been realized with an interface parallel to $\mathbf{c}_1$. The expressions of p_n and p_t are modified accordingly. The resulting values of σ obtained for different values of r or variants of the model (defined in Tab. I) are gathered in table II. Each surface tension value is the average of results given by 5 different simulations. During each simulation, pressure profiles have been averaged from time steps 40.000 to 10.000. The error represents two standard deviations in the final average of 5 points.

Table II. — *Surface tension values ; β is the angle between the interface and direction $\mathbf{c}_1$. For the model* B* *the surface tension has been maximized without modifying the equilibrium densities, as described in the present paper, using $n_0 = 4$.*

	SURFACE TENSION		
Model	range	β	σ
A	3	30°	0.20 ± 0.015
A	3	0°	0.25 ± 0.03
A	5	30°	1.00 ± 0.08
A	5	0°	1.53 ± 0.03
A	7	30°	1.92 ± 0.05
A	9	30°	2.70 ± 0.10
B	3	30°	0.32 ± 0.03
B*	3	30°	0.42 ± 0.01
C	3	30°	0.02 ± 0.03
C	3	0°	0.035 ± 0.023

It is also possible to change surface tension to some extent without modifying the equation of state : for a certain number of configurations, there are several equivalent output states for one interaction. All of them give the same momentum transfer during the interaction step. But they do not give the same contribution to $(p_n - p_t)_{\text{prop}}$ during the next propagation step.

We evaluate roughly the position of the interface with respect to the interacting pair $\mathbf{P}_k(\mathbf{x})$:

if $|n(\mathbf{x}) - n(\mathbf{x} + \mathbf{c}_k)| > n_0$ where n_0 is a reference value depending on the considered variant of the model, we assume that there is an interface between the 2 interacting sites which is more or less perpendicular to the interacting pair. Then

$$(p_n - p_t)_{\text{prop}} \simeq \sum_i N_i(\mathbf{x})[(\mathbf{c}_i \cdot \mathbf{c}_k)^2 - (\mathbf{c}_i \cdot \mathbf{c}_k^{\perp})^2]$$

if $|n(\mathbf{x}) - n(\mathbf{x} + \mathbf{c}_k)| < n_0$ we assume that the pair is either in the bulk phase or parallel to the interface. In the latter case, one gets

$$(p_n - p_t)_{\text{prop}} \simeq \sum_i N_i(\mathbf{x})\ [(\mathbf{c}_i \cdot \mathbf{c}_k^{\perp})^2 - (\mathbf{c}_i \cdot \mathbf{c}_k)^2]\,.$$

We always choose the output configuration that will maximize or minimize $(p_n - p_t)_{\text{prop}}$ depending on whether we want to increase or decrease the surface tension.

According to the results in table II, surface tension varies linearly with r (Fig. 19). The surface tension anisotropy (the ratio of fluctuations over the average) is 22 % for $r = 3$ and 41 % for $r = 5$. If we assume that Laplace's formula is valid in each point of the interface and take a sinusoidal variation for σ

$$\sigma(\theta) \simeq \sigma_0 + \sigma_1 \cos(6\,\theta)$$

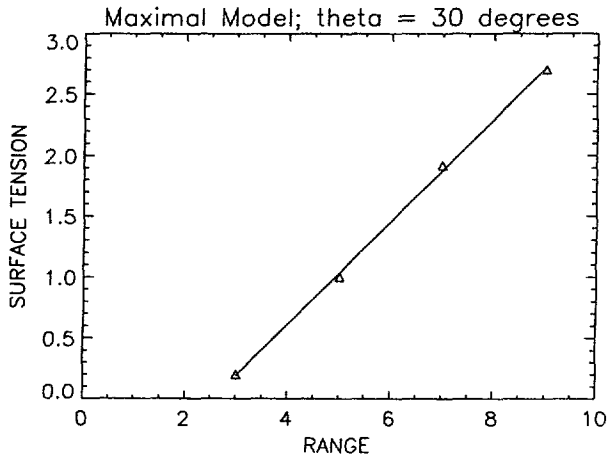

Fig. 19. — Surface tension against the interaction range, for the maximal model ; the angle β between the interface and direction $\mathbf{c}_1$ is 30°. The straight line is a least mean square fit.

then the interface $\ell(\theta)$ of a droplet in polar coordinates is

$$\ell(\theta) \simeq \ell_0 - \ell_0 \frac{\sigma_1}{35\,\sigma_0} \cos(6\,\theta).$$

We have used the expression of curvature in polar coordinates

$$\frac{1}{R} = \frac{\ell^2 + 2\,\ell'^2 - \ell\ell''}{(\ell^2 + \ell'^2)^{3/2}}$$

where $\ell' = \dfrac{d\ell}{d\theta}$. The resulting radius anisotropy $2\,\sigma_1/(35\,\sigma_0)$ is only 0.6 % for $r = 3$ and 1.2 % for $r = 5$.

7. Gibbs-Thomson relations.

In classical thermodynamics, when two phases can exchange particles, the equilibrium pressures and densities derive from the equality of chemical potentials

$$\mu_1(P, T) = \mu_2(P, T). \tag{11}$$

For the lattice-gas model, as no non-trivial energy conservation has been explicitly introduced, it is not clear *a priori* whether effective chemical potentials exist. However our numerical experiments show that equilibrium densities are unique for a given r.

Equilibrium densities have been measured during the simulations described in section 5. Results are reported in table III. It shows that the equilibrium densities can be increased or decreased very easily. However at this point we still have no way of predicting the equilibrium densities. We have checked that pressures are equal in the liquid and in the gas phases within statistical accuracy of the measurements.

In what follows we shall discuss the validity of Gibbs-Thomson relations which are usually derived from equality (11) [24]. These relations give the equilibrium pressures against the curvature $1/R$ of the interface and are of great importance for evaporation, condensation at a

Table III. — *Equilibrium densities and pressures for a flat interface ; the error is 2 standard deviations.*

EQUILIBRIUM DENSITIES AND PRESSURES					
Model	r	β	$p_{gas} \times 10^4$	gas density $\times 10^4$	liquid density $\times 10^4$
A	3	30°	407 ±2	165 ±9.4	5750 ±5
A	3	0°	408 ±3	165 ±1.6	5750 ±3
A	5	30°	59 ±2	21 ±0.8	6932 ±2
A	5	0°	68 ±2	24.2 ±0.61	6926 ±3.2
A	7	30°	15 ±1	5.1 ±0.2	7549 ±1
A	9	30°	5.1 ±0.4	1.7 ±0.15	7724 ±4
B	3	30°		1021 ±2	6115 ±2
B	3	0°		1025 ±1.5	6117 ±2
C	3	30°		2400 ±2	7620 ±1

curved interface or growth, collapse of a bubble or droplet. They determine the critical size of a nucleating droplet in a first-order phase transition. For small values of the pressure difference ΔP across the interface the Gibbs-Thomson relations read

$$p_1 = p_0 + \Delta p \frac{\rho_1}{(\rho_1 - \rho_2)}$$
$$p_2 = p_0 + \Delta p \frac{\rho_2}{(\rho_1 - \rho_2)} \tag{12}$$

where p_0 is the equilibrium pressure for a flat interface and $\Delta p = p_1 - p_2$. We note with subscripts 1 and 2 quantities associated with each phase. Subscript 1 refers to the inner fluid.

When the curvature $1/R$ is small and the velocity of the interface is negligible, an explicit form may be obtained by using Laplace's law $p_1 - p_2 = \sigma/R$:

$$p_1 = p_0 + \frac{\sigma}{R} \frac{\rho_1}{(\rho_1 - \rho_2)}$$
$$p_2 = p_0 + \frac{\sigma}{R} \frac{\rho_2}{(\rho_1 - \rho_2)} \tag{13}$$

We attempted to measure pressures inside and outside droplets of the dense phase. The liquid and gas pressures and the density profile have been averaged on at least 24 000 time steps. The density d is measured as a function of the distance to the center of the droplet. Care is taken to account for the Brownian motion of the droplet : the center of the droplet is recomputed at each time step. The radius R of the bubble is defined by $d(R) = (d_1 - d_2)/2$. Measurements for $r = 3$ yield poor results, mainly due to large fluctuations in the droplet shape. This is not unexpected, as the $r = 3$ model is close to the critical point (see Tab. II). The $r = 5$ model yields a linear relation between the liquid pressure and $1/R$. Results for the gas pressure are poor, due to the very low gas density for this model. Thus while Laplace's law may be checked, it is not possible to obtain a satisfactory test of the full Gibbs-Thomson relations (13). Figure 20 shows the gas and liquid pressures *versus* $1/R$. The linearity is well verified for $R > 33$. At the same time, we check the validity of Laplace's formula. For small radii, we observe the expected divergence from Laplace's formula. For large radii we expect convergence of $R\,\Delta p$ to σ. This convergence is much slower than in the two-color ILG [11] ($1/R_c \geq 0.06$). However, as shown in figure 21, the measured values of $R\,\Delta p$ may be

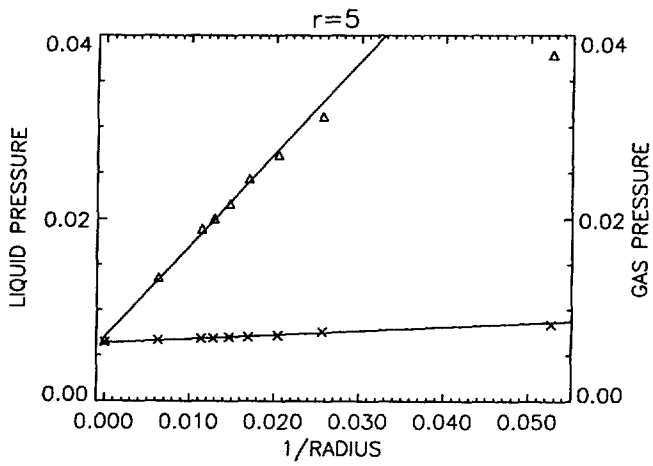

Fig. 20. — Gas and liquid pressure against $1/R$, for $r = 5$.

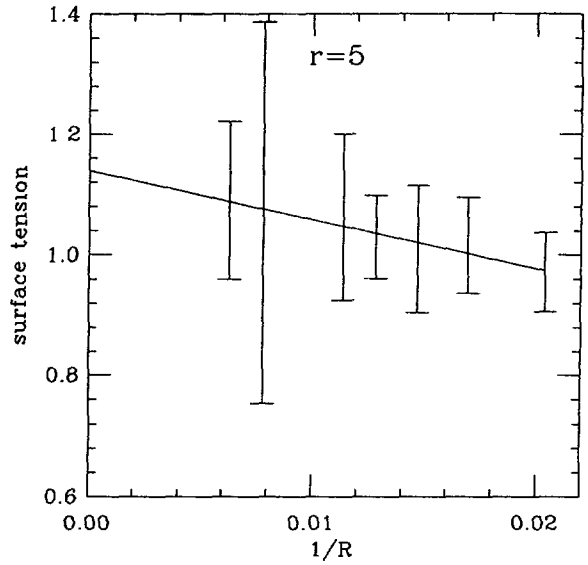

Fig. 21. — Values of the surface tension deduced from Laplace's formula plotted against $1/R$. The full line results from a least mean square fit.

extrapolated using a least square fit to $\sigma = 1.14 \pm 0.16$. There is a good agreement, within statistical error bars, with the value obtained in section 5.

Better fits to the p_i *vs.* $1/R$ relations may be obtained if the fluctuating interface at $r = 3$ is pinned to a wall. In reference [15] an experiment in a capillary tube was performed. The geometry of the experiment is shown in figure 22. Solid walls are added in a standard fashion, letting particles bounce back into the direction they come from on solid sites. The interactions between solid sites and non-solid sites follow simple rules : the maximum possible momentum **t**, pointing towards the solid site, is added to the fluid site. This rule results in the merging of the interface with a finite contact angle θ. We refer the interested reader to

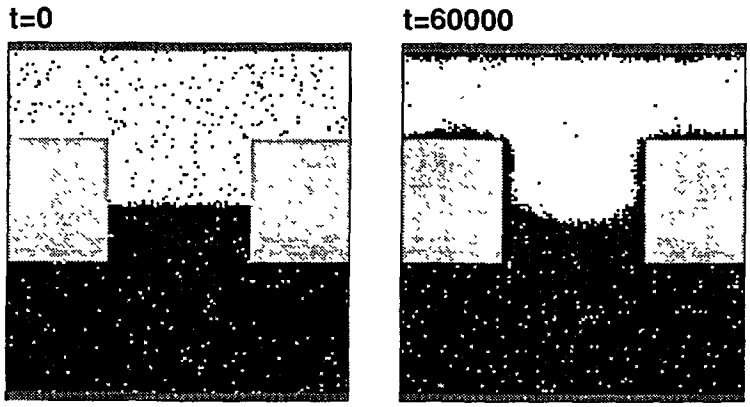

Fig. 22. — An experimental setup for capillary pressure measurement in a capillary tube. The equilibrium pressures of liquid and gas are measured above and below the meniscus. From reference [15].

reference [15] for a discussion of the contact angle measurement. In reference [15] a linear dependence of the pressures with the contact angle was found. However, this dependence is not as given by equations (13). To account for the discrepancy, it is necessary to introduce a new coefficient α. The modified Gibbs-Thomson relations become

$$\left.\begin{aligned} p_1 &= p_0 + \left(1 - \alpha \frac{\rho_2}{\rho_2 - \rho_1}\right)(p_1 - p_2) \\ p_2 &= p_0 - \alpha \frac{\rho_2}{\rho_2 - \rho_1}(p_1 - p_2) \\ p_1 - p_2 &= \frac{\sigma \cos\theta}{R'} \end{aligned}\right\} \tag{14}$$

where $R' = R/\cos\theta$ is the capillary half-width. The measured pressures are shown in figure 23. The best fit is obtained for $\alpha = 1.34 \pm 0.01$ and $\sigma \cos\theta = 0.21 \pm 0.02$. Direct measurements of θ were also performed by fitting the meniscus shape. They yield $\theta = 22 \pm 8$ in degrees. The last three measurements are again compatible with the values of σ obtained in section 5.

8. Hydrodynamical behavior.

Because the basic rules of our model are much more complex than those of the non-interacting lattice gas, a full derivation of the hydrodynamic equations of our model seems a daunting task. However, basic symmetries and conservation laws of our model suggest that we recover, on the large scale, a set of equations that mimics those of an incompressible fluid with a free liquid-vapor interface. In the bulk of each phase the symmetries of fourth order tensors [22] impose a Navier-Stokes like equation. Such an equation has indeed been derived for the minimal model of reference [20] :

$$\begin{aligned} \partial_t \rho u_\alpha + \partial_\beta (g(\rho)\, u_\alpha\, u_\beta) = &- \partial_\alpha p(\rho, u^2 ; r) + \partial_\beta [\nu(\rho ; r)\, \partial_\beta \rho u_\alpha] \\ &+ \partial_\alpha \left[\left(\frac{D-2}{D} \nu(\rho ; r) + \zeta(\rho ; r) \right) \partial_\beta \rho u_\beta \right]. \end{aligned} \tag{15}$$

The coefficient $g(\rho)$ is characteristic of the lack of Galilean invariance of the model. We have

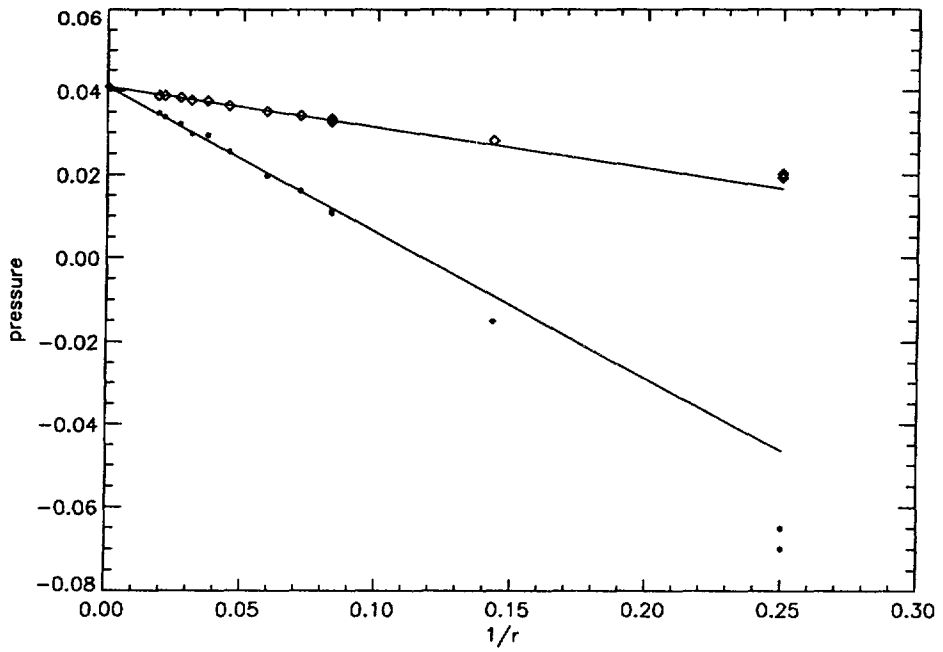

Fig. 23. — Results of experiment in capillary tube. Liquid and gas equilibrium pressures as a function of half capillary width are shown. Diamonds represent gas pressure and circles liquid pressure. The straight lines indicate a fit to equation (14). From reference [15].

not calculated it for our model, but it is obtained for the minimal model. We also have a mass conservation equation

$$\partial_t \rho + \operatorname{div} \rho \mathbf{u} = 0 . \tag{16}$$

As usual in compressible gas dynamics we expect to recover the incompressible hydrodynamic limit for small Mach numbers $M = u/c$, as in the non-interacting gas :

$$\frac{\partial u}{\partial t} + (u \,.\, \nabla)\, u = -\nabla p + \nu \nabla^2 u \tag{17}$$

and

$$\operatorname{div} \mathbf{u} = 0 . \tag{18}$$

In what follows, we investigate shear wave modes predicted by this equation numerically. However, before turning to these numerical simulations, let us consider conditions on interfaces between liquid and gas densities. Conditions on an interface with a possible phase change are as follows. We will denote by subscripts 1 and 2 quantities associated with each phase, and for any quantity X, $[X] = X_2 - X_1$ will be the jump of X across the interface. The normal $\mathbf{n}$ to the interface will be oriented from 1 to 2, and the interface velocity U_I will be positive if the interface moves from 1 to 2. In the real world, we have continuity of tangential velocities :

$$[\mathbf{u} \cdot \mathbf{t}] = 0 \tag{19}$$

where $\mathbf{t}$ is a tangent vector to the interface. We have not set up numerical experiments to investigate such tangential jump conditions. Because of the lack of Galilean invariance of our model, we may have instead

$$\mathbf{u}_1 \mathbf{t}_1 = K(r)\, \mathbf{u}_1 \mathbf{t}_1 . \tag{20}$$

Mass conservation imposes the following necessary conditions both in the real world and in our model :

$$[\rho \mathbf{u} \cdot \mathbf{n}] = [\rho]\, U_I . \tag{21}$$

Momentum conservation similarly imposes a jump condition on the normal component of momentum flux, which reads

$$[S_{\alpha\beta}\, n_\beta] = n_\alpha \left(\frac{\sigma}{R'} + \frac{\sigma}{R''} \right) \tag{22}$$

where

$$S_{\alpha\beta} = p\delta_{\alpha\beta} + \nu\rho\, (\partial_\beta u_\alpha + \partial_\alpha u_\beta) \tag{23}$$

and where R', R'' are the radii of curvature of the interface. Since changes of phase are possible, one also needs to impose equality of chemical potentials $\mu(T, p)$ across the interface, as expressed in equation (11). When $p - p_{eq}$ is small and $\mathbf{u} = 0$, equations (11) lead to equations (12) above. We have not yet performed numerical experiments to determine directly the validity of these relations in the presence of fluid flow near the interface.

An interesting question is whether it is possible to rescale our model in such a way that one would recover the full real world equations, with $g(\rho_G) = g(\rho_L) = K = \alpha = 1$. A quick counting of the possible transformations of space, time, and mass shows that it is impossible. On the other hand, for special problems, such as a vanishing gas density or a vanishing velocity in one of the phases, a mapping on the realistic equations is possible.

Numerical experiments on shear waves were performed with two purposes in mind : to verify the validity of equation (15) and to obtain a measurement of the viscosity for various variants of the model. We initialize the fluid with a sine-wave velocity field : $u_1(\mathbf{x}, t) = A_0 \sin(2\pi x_2/\lambda)$, $u_2 = 0$. We then observe the decay of the amplitude $A(t)$ of the shear wave. The amplitude of the sine wave is actually obtained after averaging 256 amplitudes until a maximal time T, and a fit to exponential decay is made (see Fig. 25 for an example). This fit yields an estimate of the viscosity. The experiments are then repeated a number of times between 2 and 5 and the error is estimated.

At short wavelengths λ we observe a small elastic effect : the amplitude changes sign before decaying to 0 (Fig. 24). At longer wavelengths this effect is not seen (Fig. 25). A good agreement is seen with an exponential decay. The measurements of viscosity converge well with increasing λ (Fig. 26). We performed systematic measurements with varying r which show an approximate r^2 dependence at large r (Fig. 27). The resulting measurements of viscosity are shown in table IV.

9. An example of application : soap froth.

To illustrate another possible application we attempted to simulate the formation of 2D soap froth on surfaces, such as in Langmuir film experiments [27]. We perform a spinodal decomposition on a $240 \times 240\ \sqrt{3}/2$ lattice as often described in this and other [1, 2] papers. However during the simulation we removed particles at a constant rate. About 300 particles are

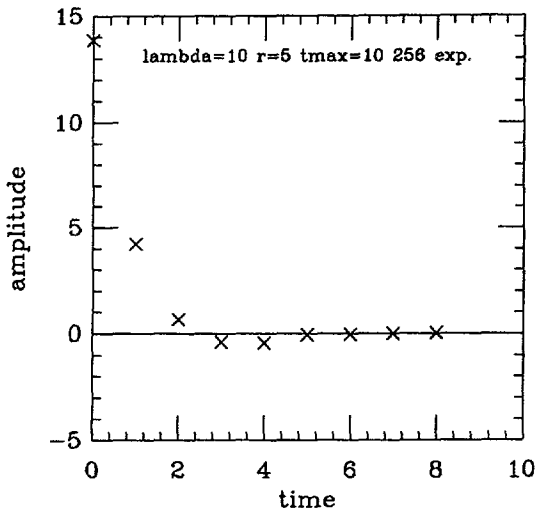

Fig. 24.

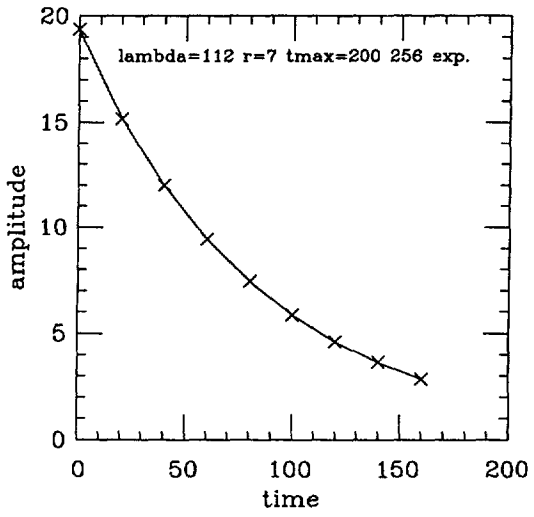

Fig. 25.

Fig. 24. — Decay of sine wave amplitude for short wavelengths.

Fig. 25. — Decay of sine wave amplitude for long wavelengths.

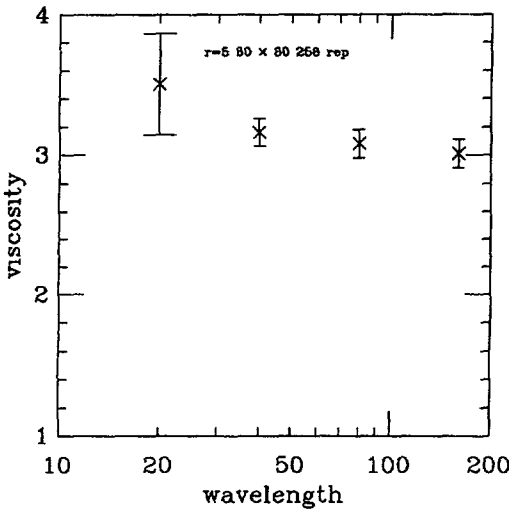

Fig. 26.

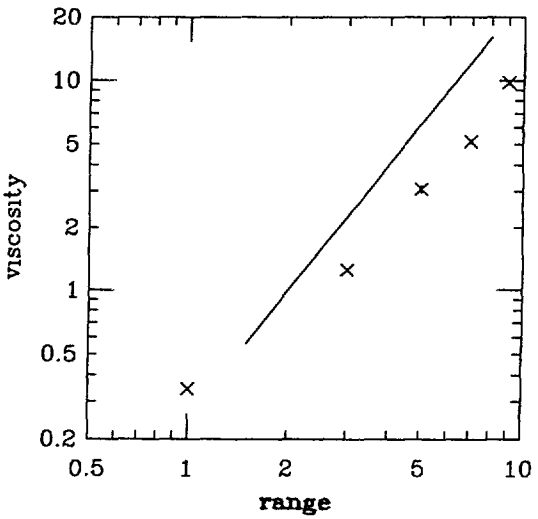

Fig. 27.

Fig. 26. — Variation of viscosity with wavelength λ.

Fig. 27. — Variation of viscosity with interaction range r.

removed at each time step. This corresponds to the dissolving of molecules into the bulk water phase in Langmuir films. The resulting patterns are shown in figure 28 which illustrates the ability of the model to simulate liquid films. The state reached at time $t = 440$ is unstable and the system evolves towards a cellular structure similar to those obtained in experiments on soap froths.

Table IV. — *Measured values of the viscosity for some of the variants.*

model	r	λ/r	ν_L	ν_G
A	3	16	1.25±0.1	-
A	5	16	3.08±0.1	-
A	7	16	5.15±0.1	-
A	9	16	9.8±0.05	-
A	3	32	1.30±0.2	1.192±0.1
B	3	16	1.17 ±0.04	-
C	3	16	1.69 ±0.2	0.67±0.04

10. Conclusion.

Although the model is microscopically irreversible we did find most features expected for the large scale dynamics and thermodynamics of interfaces. Laplace's law is observed as expected from simple mechanical arguments. The Gibbs-Thomson relations are not verified, which is apparently a signature of microscopic irreversible behavior. However, the linear dependence of the equilibrium pressures with the capillary pressure drop ensures agreement with classical thermodynamics. In particular the positivity of the correcting factor α is of importance for the obtention of correct phase transition dynamics. Viscous effects are properly represented at the large scale.

In spite of its potential for applications, this study remains incomplete in several respects. It may be useful to have a short list of these shortcomings :

(i) We do not have a full hydrodynamical picture of the model, neither theoretical nor numerical. An important missing item is the behavior of a sheared interface as described by equations (20).

(ii) We do not know what the non-Galilean coefficients $g(\rho)$ are for the maximal model. It is likely that things improve with the minimal model where simple calculations yield $g(\rho)$ easily. But no model with $g(\rho) = 1$ has been found yet.

(iii) We do not have a picture of the *fluctuating* hydrodynamics of our model. It would be interesting to put these hydrodynamics in a Langevin equation form, and to investigate the difference with classical formalism.

(iv) We have not investigated the neighborhood of the liquid-gas critical point. There we expect that the analysis and the numerics would reveal interesting features such as critical exponents that would violate universality.

(v) We have some evidence of a 2nd phase transition near $r = 9$. This transition appears as spatial, steady state density fluctuations of period close to, but not commensurate with, r.

We expect to be able to address these questions using the minimal interaction model of reference [20]. We hope that the model or rather one of its variants will then be a useful tool for simulations of the kind of phenomena already mentioned : coalescence, flow in porous media, soap froths, etc. It has already been used for the study of interfaces in porous media [15, 16]. For these applications, the choice of the appropriate model is a tricky issue :

(i) At $r = 3$ the model is relatively close to the liquid gas critical point and suffers from a low surface tension. This makes interface fluctuations very large.

(ii) At larger values of r viscosity increases rapidly and we eventually reach the 2nd transition mentioned above. Moreover, as r increases the gas density decreases considerably. The lattice gas then becomes inefficient for simulations of flow in the gas phase.

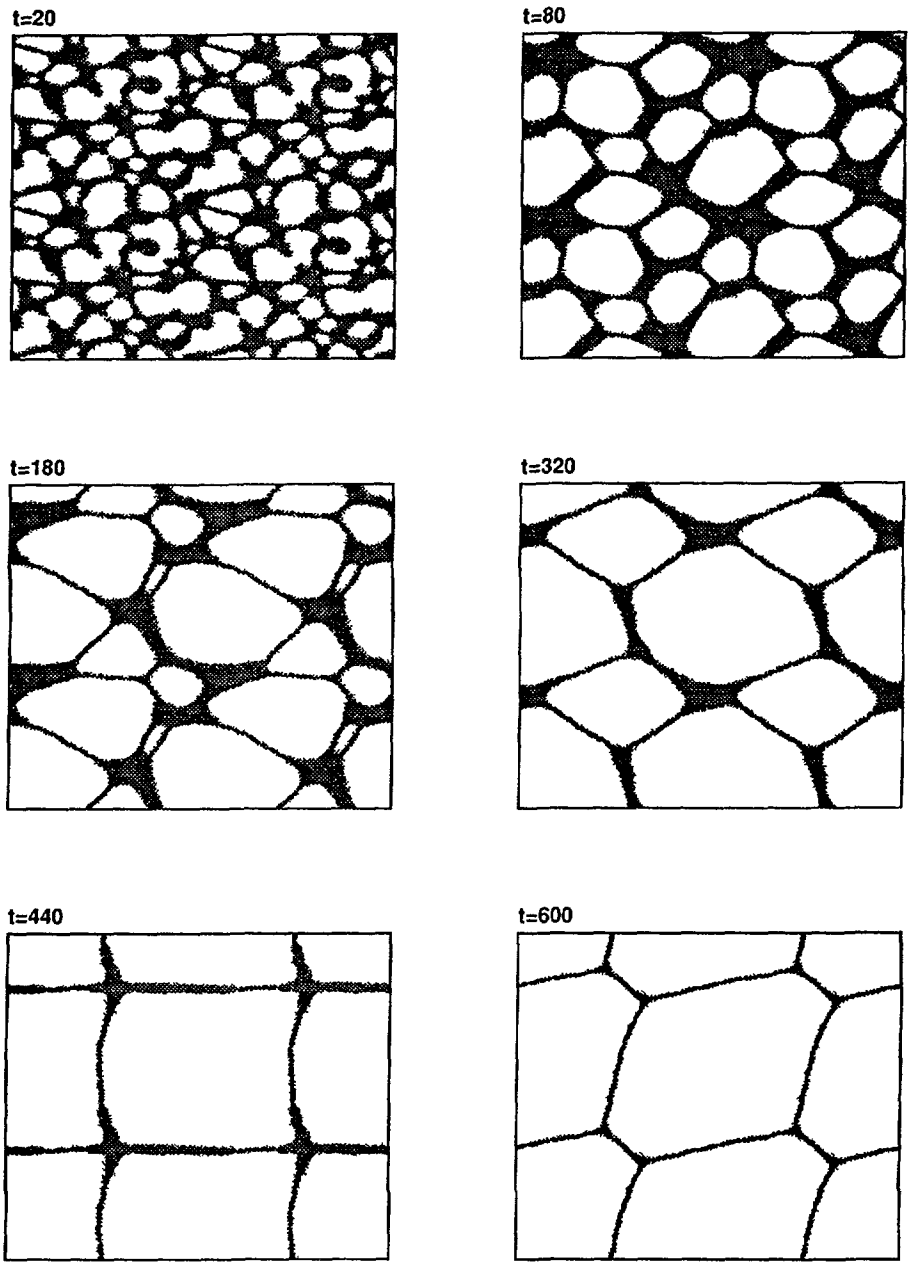

Fig. 28. — Spinodal decomposition with particle removal. The lattice is initialised with a uniform density $d = 0.3$. We have used model A with $r = 5$. Boundary conditions are periodic. The same picture has been represented four times to make the visualisation easier.

In our experience, the optimal choice for r seems to lie between 3 and 5. In some cases a desirable feature of the simulation is a low capillary number $Ca = \eta U/\sigma$, where U is a typical velocity. This velocity cannot be made much smaller than 1 without a great loss of efficiency. Thus the scalings found in sections 5 and 7 ($\sigma \sim r$ and $\eta \sim r^2$) yield $Ca \sim r$. This indicates again that small values of r may be optimal.

Acknowledgments.

We thank Valerie Pot for contributing figures 22 and 23. Laboratoire de Physique Statistique is supported by CNRS and Universities of Paris 6 and 7.

Appendix A :

Collisions rules.

We refer the reader to the paper of d'Humières and Lallemand [23] to get the full list of collision rules for the FHP III model. We shall use their notation in what follows. We just list below the rules we have actually used in our simulations when they are different from the FHP III ones :

$$A_{520}(j \to k) = 0 .$$
$$A_{320}(1 \to k) = 0,\ k = 2 \text{ or } 3 .$$
$$A_{320}(j \to 1) = 0,\ k = 2 \text{ or } 3 .$$
$$A_{420}(1 \to k) = 0,\ k = 2 \text{ or } 3 .$$
$$A_{420}(j \to 1) = 0,\ k = 2 \text{ or } 3 .$$

Appendix B :

Further information on the choice of pairs.

The definition of « even » pairs given in the main text assumes that $\mathbf{x}_{00}$ is a reference point for rotations of the lattice. In fact, as boundary conditions are periodic, there is no reason to choose this point rather than another one. Indeed in our simulations the reference point was randomly chosen at each time step. We show below that there are only four independent choices.

Pairs in direction $\mathbf{c}_1$ have been defined as indicated in figure 29. As the resulting pattern is periodic with a period 2 in the x and y directions, translations of it generate only four different sets of pairs.

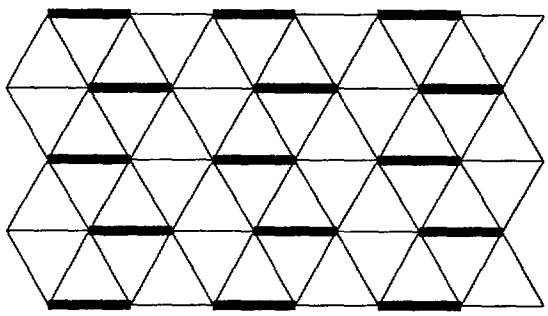

Fig. 29. — Definition of pairs in direction $\mathbf{c}_1$.

Pairs in directions $\mathbf{c}_2$ and $\mathbf{c}_3$ are obtained from the above pattern by $\frac{\pi}{3}$ and $\frac{2\pi}{3}$ rotations respectively. A more thorough study shows that the whole set of pairs (the superposition of pairs in the three directions) can form only four different patterns that cannot be reduced to one another by a translation. Two of them have been represented in figure 30. Two others are obtained from the former ones by rotations of π.

Each pattern has a $4 \times 4 \times \sqrt{3}/2$ basic mesh in lattice units, so it can be mapped on the lattice in sixteen different ways. All of them must be explored during a simulation. Therefore, when interactions are performed in one direction, one set of pairs is randomly chosen among the four possible ones. Indeed, if the position of pairs were always the same, we would not only create inhomogeneities ; but the definition of pairs would give only one of the four full patterns of figure 30. The model would be subdivided into four variants, each of them corresponding to one of the four patterns.

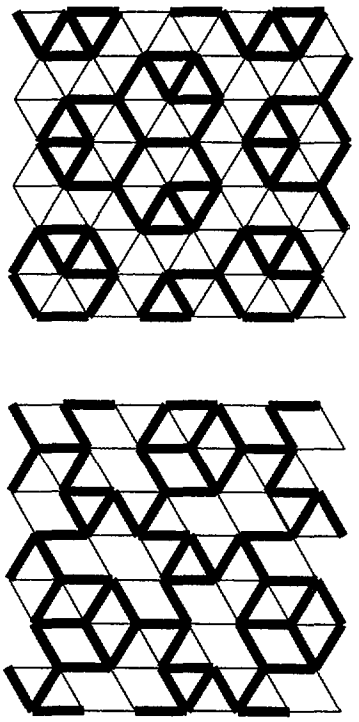

Fig. 30. — Resulting patterns obtained by the superposition of pairs in the three directions.

Appendix C :

Viscosity — Calculation « à la Maxwell ».

We consider a steady laminar, pure shear flow : $\mathbf{U} = U_x(y)\,\mathbf{e}_x$. The viscous shear stress can be written, on the one hand, as

$$\sigma_{xy} = \nu\rho \frac{\partial U_x}{\partial y}$$

and, on the other hand, as

$$\sigma_{xy} = - \overline{\mathbf{M}_{xy} v_y}$$

where $\mathbf{M}_{xy}$ is the instantaneous x-momentum transfer along the y direction per unit time and area and v_y the velocity of this transfer. Here, the overbar represents an average taken over a large number of molecules.

Let us evaluate the part of the viscosity due to the interaction. We will consider only the first interaction given in figure 4. The probability p_i ($i = 2$ or 3) of having an interaction between the particles of site $\mathbf{x}$ and those of site $\mathbf{x}' = \mathbf{x} + r\mathbf{c}_i$ is

$$p_i = N_i(\mathbf{x}') \, [1 - N_{i+3}(\mathbf{x}')] \, [1 - N_i(\mathbf{x})] \, N_{i+3}(\mathbf{x}) \, .$$

Here, N_i is the probability of having the state i occupied :

$$N_i = N_i^{eq} + N_i^{(1)} + \cdot$$

where N_i^{eq} is the Fermi-Dirac equilibrium distribution ($d = \rho/7$ is the reduced density) :

$$N_i^{eq} = d \left(1 + \frac{7}{3} \mathbf{u} \cdot \mathbf{c}_i + \cdot \quad \right)$$

and $N_i^{(1)}$ is the correction at first order in velocity gradients. According to reference [22], we take

$$N_i^{(1)} = (1 + \lambda) \, \psi d Q_{i\alpha\beta} \frac{\partial U_\alpha}{\partial x_\beta} = (1 + \lambda) \, \psi d C_{ix} C_{iy} \frac{\partial U_x}{\partial y}$$

(as we consider distributions after the collision step, the expression has been multiplied by $(1 + \lambda)$ where λ is the eigenvalue of the linearised collision matrix associated with the eigenvector $Q_{i\alpha\beta}$. We assume the density to be constant at the considered order). A short calculation gives

$$p_i = d^2(1 - d)^2 + (1 + \lambda) \, \psi d^2(1 - d)(1 - 2d) \frac{\partial U_x}{\partial y} C_{ix} C_{iy} + d^2(1 - d) \, ar \frac{\partial U_x}{\partial y} C_{ix} \, .$$

Then $\mathbf{M}_{xy} = - \sum_{i = 2, 3} 2 p_i C_{ix}$ and the velocity of the transfer is rC_{iy}. It obtains

$$\nu = Ad(1 - d) r^2 + Bd(1 - d)(1 - 2d)(1 + \lambda) \, \psi r \, .$$

At the dominant order, ν is proportional to r^2.

References

[1] APPERT C. and ZALESKI S., Lattice Gas with a Liquid-gas Transition, *Phys. Rev. Lett.* **64** (1990) 1-4.

[2] APPERT C., ROTHMAN D. H. and ZALESKI S., A Liquid-gas Model on a Lattice, *Physica D* **47** (1991) 85-96.

[3] HYMAN J. M., Numerical Methods for Tracking Interfaces, *Physica 12 D* (1984) 396-407.

[4] GLIMM J., MC BRYAN O., MENIKOFF R. and SHARP D. H., Front tracking applied to Rayleigh Taylor instability SIAM, *J. Sci. Stat. Comput.* **7** (1986) 230-251.

[5] HIRT C. W. and NICHOLLS B. D., Volume of Fluid (VOF) Method for the Dynamics of Free Boundaries, *J. Comp. Phys.* **39** (1981) 201-225.

[6] LAFAURIE B. and ZALESKI S., Front capturing for flows with surface tension : Volume Of Fluid revisited, in preparation.

[7] KOPLIK J. and BANAVAR J. R., Molecular Dynamics of Interface rupture, preprint.

[8] BROCHARD F., Stabilité d'un ruban de liquide déposé sur un support liquide, *C.R.A.S. Paris Série II* **311** (1990) 295-300.

[9] FRISCH U., HASSLACHER B. and POMEAU Y., Lattice-gas automata for the Navier-Stokes equation, *Phys. Rev. Lett.* **56** (1986) 1505-1509.

[10] APPERT C., POT V. and ZALESKI S., Les liquides analogiques sur réseau, *Bull. Soc. Fr. Phys.* **83** (1992) 8.

[11] ROTHMAN D. H. and KELLER J. M., Immiscible Cellular-Automaton Fluids, *J. Stat. Phys.* **52** (1988) 1119.

[12] BONETTI M., NOULLEZ A. and BOON J.-P., Cellular Automata and the Modeling of Complex Physical Systems, P. Manneville, N. Boccara, G. Vichniac and R. Bidaux Eds. (Springer, Berlin, 1989) p. 239.

[13] D'HUMIÈRES D. LALLEMAND P. and SEARBY G., Numerical Experiments on Lattice Gases : Mixtures and Galilean Invariance, *Complex Systems* **1** (1987) 632.

[14] CLAVIN P., LALLEMAND P., POMEAU Y. and SEARBY J., Simulation of free boundaries in flow systems by lattice-gas models, *J. Fluid Mech.* **188** (1988) 437-464.

[15] POT V., APPERT C., MELAYAH A., ROTHMAN D. H. and ZALESKI S., Modelling water flow in unsaturated porous media by interacting lattice gas-cellular automata : I. Evaporation preprint, submitted to *Water Research Resources.*

[16] DI PIETRO L., MELAYAH A. and ZALESKI S., Modelling water flow in unsaturated porous media by interacting lattice gas-cellular automata : II Infiltration preprint, submitted to *Water Research Resources.*

[17] GUNSTENSEN A. K., ROTHMAN D. H., ZALESKI S. and ZANETTI G., Lattice Boltzmann model of immiscible fluids, *Phys. Rev. A* **43** (1991) 4320.

[18] CREUTZ M., Deterministic Ising Dynamics, *Ann. Phys. (NY)* **167** (1986) 62-72.

[19] ROTHMAN D. H. and ZALESKI S., Spinodal Decomposition in a Lattice Gas Automaton, *J. Phys. France* **50** (1989) 2167.

[20] APPERT C., D'HUMIÈRES D. and ZALESKI S., Lattice Gas with Minimal Interactions, *CRAS* Série II **316** (1993) 1-0 ; Three Dimensional Lattice Gas with Minimal Interactions, submitted to Transport Theory and Statistical Physics, Proceedings of Euromech 287, Discrete Models in Fluid Dynamics.

[21] ZANETTI G., Hydrodynamics of Lattice-Gas Automata, *Phys. Rev. A* **40** (1989) 1539-1548.

[22] FRISCH U., D'HUMIÈRES D., HASSLACHER B., LALLEMAND P., POMEAU Y. and RIVET J.-P., Lattice Gas Hydrodynamics in Two and Three Dimensions, *Complex Systems* **1** (1987) 648.

[23] D'HUMIÈRES D. and LALLEMAND P., Numerical Simulations of Hydrodynamics with Lattice Gas Automata in Two Dimensions, *Complex Systems* **1** (1987) 599.

[24] ROCARD Y., Thermodynamique (Masson, Paris, 1952) p. 62.

[25] LANDAU and LIFSHITZ, Course of Theoretical Physics, Vol. **10,** Physical Kinetics (Pergamon Press, 1981).

[26] ROWLINSON and WIDOM, Molecular Theory of Capillarity (Clarendon Press, Oxford, 1982).

[27] BERGE B., SIMON A. J. and LIBCHABER A., Dynamics of gas bubbles in monolayers, *Phys. Rev. A* **41** (1990) 6893-6900.